MurD ligase from E. coli : Tetrahedral intermediate formation study by hybrid quantum mechanical/molecular mechanical replica path method

ARTICLE *in* PROTEINS STRUCTURE FUNCTION AND BIOINFORMATICS · FEBRUARY 2009

Impact Factor: 2.63 · DOI: 10.1002/prot.22188 · Source: PubMed

3 AUTHORS, INCLUDING:

Andrej Perdih
National Institute of Chemistry
44 PUBLICATIONS **440** CITATIONS
SEE PROFILE

Tom Solmajer
National Institute of Chemistry
98 PUBLICATIONS **1,244** CITATIONS
SEE PROFILE

PROTEINS
STRUCTURE ■ FUNCTION ■ BIOINFORMATICS

MurD ligase from *E. coli*: Tetrahedral intermediate formation study by hybrid quantum mechanical/molecular mechanical replica path method

Andrej Perdih, Milan Hodoscek, and Tom Solmajer*

Laboratory for Molecular Modeling and NMR Spectroscopy, National Institute of Chemistry, Hajdrihova 19, 1001 Ljubljana, Slovenia

ABSTRACT

MurD (UDP-*N*-acetylmuramoyl-L-alanine:D-glutamate ligase), a three-domain bacterial protein, catalyses a highly specific incorporation of D-glutamate to the cytoplasmic intermediate UDP-*N*-acetyl-muramoyl-L-alanine (UMA) utilizing ATP hydrolysis to ADP and P_i. This reaction is part of a biosynthetic path yielding bacterial peptidoglycan. On the basis of structural studies of MurD complexes, a stepwise catalytic mechanism was proposed that commences with a formation of the acyl-phosphate intermediate, followed by a nucleophilic attack of D-glutamate that, through the formation of a tetrahedral reaction intermediate and subsequent phosphate dissociation, affords the final product, UDP-*N*-acetyl-muramoyl-L-alanine-D-glutamate (UMAG). A hybrid quantum mechanical/molecular mechanical (QM/MM) molecular modeling approach was utilized, combining the B3LYP QM level of theory with empirical force field simulations to evaluate three possible reaction pathways leading to tetrahedral intermediate formation. Geometries of the starting structures based on crystallographic experimental data and tetrahedral intermediates were carefully examined together with a role of crucial amino acids and water molecules. The replica path method was used to generate the reaction pathways between the starting structures and the corresponding tetrahedral reaction intermediates, offering direct comparisons with a sequential kinetic mechanism and the available structural data for this enzyme. The acquired knowledge represents new and valuable information to assist in the ongoing efforts leading toward novel inhibitors of MurD as potential antibacterial drugs.

Proteins 2009; 74:744–759.

Key words: QM/MM; MurD; replica path method; modeling of enzyme reactions; ATP driven amide bond synthesis; biomolecular simulations.

INTRODUCTION

The biosynthesis of peptidoglycan, an essential bacterial cell-wall polymer unique to prokaryotic cells, outlines a complex multistage process divided into the early stages of intracellular assembly of the UDP-MurNAc pentapetide, a translocation step on the extracellular side and a subsequent incorporation into the nascent biopolymer.[1] A properly constructed peptidoglycan provides rigidity, flexibility, and strength that are indispensable for bacterial cells to grow and divide while withstanding high internal osmotic pressure.[2] Among various enzymes that form the cornerstones of this sophisticated process, four structurally and functionally similar ADP-forming ligases (Mur ligases) termed MurC, MurD, MurE, and MurF, catalyze the intracellular assembly of the peptide moiety by the consecutive addition of L-Ala, D-Glu, *meso*-DAP (or L-Lys), and D-Ala-D-Ala to the starting UDP-precursor (UDP-MurNAc).[3] Since peptidoglycan represents an optimal target with respect to selective toxicity, unexploited targets within the pathway (e.g. Mur ligases) are recently being intensively studied to provide novel effective antibacterial drugs to overcome the increasing emergence of bacterial resistance to most of the known antibiotics.[4,5]

The Mur ligase family is outlined as prime example of modular structure in protein architecture with molecules made up of three domains or modules allowing successful molecular recognition of the specific UDP-substrate (UDP-*N*-acetylmuramoyl group).[3] The N-terminal domain is primarily responsible for the binding of the UDPMurN-Ac substrate (e.g., UMA, UMAG, UMAN etc), a central domain which bears resemblance to the ATP binding domains of a number of ATPases and GTPases and a C-terminal domain which is assumed to be involved in the binding of the incoming condensing amino acid [Fig. 1(A)].[3] The available assortment of

Additional Supporting Information may be found in the online version of this article.
Grant sponsor: Ministry of Higher Education, Science and Technology of the Republic of Slovenia.
*Correspondence to: Tom Solmajer, National Institute of Chemistry, Hajdrihova 19, 1001 Ljubljana, Slovenia. E-mail: tom.solmajer@ki.si
Received 10 April 2008; Revised 8 June 2008; Accepted 16 June 2008
Published online 14 August 2008 in Wiley InterScience (www.interscience.wiley.com).
DOI: 10.1002/prot.22188

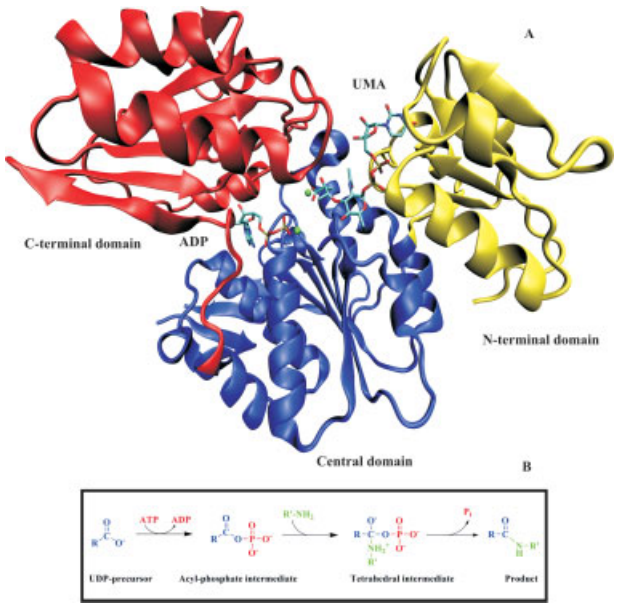

Figure 1

A: Protein structure of the closed conformation of *E. coli* MurD (PDB code:2UAG)[6] used in QM/MM calculations. The N-terminal domain is denoted in yellow, the central domain in blue and the C-terminal domain in red. The experimentally determined positions of ADP, UMA, and both magnesium ions are also displayed (**B**) Scheme of the general Mur ligase reaction mechanism: The starting UDP precursor first reacts with ATP to yield the acyl-phosphate intermediate. Afterwards, an addition of the incoming amino acid results in a tetrahedral intermediate. Finally, a dissociation of the phosphate group from the tetrahedral intermediate gives the final product—a new UDP precursor elongated by the condensing amino acid.

solved crystal structures revealed that substantial conformational changes, especially in the connecting loop between the C-terminal and central domain, enable several distinct positions of the C-terminal domain.[3]

In seminal biochemical investigations of the MurC and MurF enzymes' kinetic mechanism substrate, the binding order has been established, starting with the binding of ATP followed by the UDP-precursor and concluding by the binding of the condensing amino acid.[7,8] Kinetic studies also suggested a sequential catalytic mechanism.[7,8] As schematically presented in Figure 1(B) the first step involves the activation of the UDP precursor's carboxylic group by forming the acyl-phosphate intermediate whose existence has been established by various biochemical experiments.[9,10] In the next catalytic step the nucleophilic amino group of the condensing amino acid residue attacks the activated terminal carbonyl carbon, which results in a tetrahedral intermediate formation. Finally, the dissociation of a phosphate group provides a new UDP precursor elongated by the incoming amino acid. A similar enzymatic mechanism of amide bond formation driven by ATP hydrolysis is encountered in nature in glutamine synthetase,[11] D-alanine-D-alanine ligase,[12] glutathion synthetase,[13] γ-glutamylcysteine synthetase,[14] and folylpoly-γ-L-glutamate synthetase, an enzyme structurally very similar to bacterial ligases and belonging to the same ADP-forming ligase superfamily.[15]

MurD (UDP-*N*-acetylmuramoyl-L-alanine:D-glutamate ligase) is the second enzyme in the bacterial ligase series and catalyses a highly specific incorporation of D-glutamate to the cytoplasmic intermediate UDP-*N*-acetyl-muramoyl-L-alanine (UMA) concomitant with a degradation of ATP to ADP and P_i. X-ray structural studies of MurD from bacterial species *E. coli* by Dideberg and co-workers resulted in several MurD crystal structures, providing detailed information regarding the enzyme active conformation as well as the positions and binding patterns of ligands UMA, ADP (PDB: 2UAG and 3UAG) depicted in Figure 1(A) and the product UMAG (PDB: 4UAG).[6] Subsequent structural studies revealed two additional "open" structures of MurD (PDB: 1EEH and 1E0D) bearing two distinct positions of the C-terminal domain.[16] To gain insight into UMA and ATP binding along with the closing motion of the C-terminal domain, Targeted Molecular Dynamics (TMD) simulations studies were initiated to propose two dynamic models of the closing process.[17]

On the basis of the X-ray structural data that included modeling of the γ-ATP phosphate moiety, the atomistic details of the *E. coli* MurD enzymatic mechanism were proposed as outlined schematically in Figure 2.[6] Additionally, site-directed mutagenesis studies of 14 MurD ligase residues were performed, inspecting primarily the residues conserved in all Mur synthetases, and their role was evaluated by measuring their steady-state kinetics.[18] In a generally accepted bacterial ligase catalytic model, the first step involves the activation of the UMA carboxylic group by forming the acyl-phosphate intermediate. Existence of the acyl-phosphate chemical species in the case of MurD was proven experimentally by borohydride trapping experiments.[9] The S_N2 nucleophilic substitution mechanism was suggested where the migrating γ-phosphate group passes through a bipyramid-like transition state to yield the acyl-phosphate species. Two magnesium ions, together with Lys115 located between the β and γ-phosphate, were presumed to neutralize the charge repulsion of both reacting species, thereby facilitating γ-phosphate transfer and stabilizing the obtained intermediate.[6] Site directed mutagenesis of Lys115 to Ala115 showed a dramatic decrease in enzyme activity compared with a wild-type enzyme, giving additional support to a significant role of this residue.[18] The next step of the MurD reaction commences when a nucleophilic amino group of D-Glutamate reacts with the UMA activated terminal carbonyl carbon, resulting in a tetrahedral intermediate formation. During the C—N covalent bond formation a catalytic base is required to accept the proton from the charged D-Glu amine. Several possibilities for this catalytic steps were considered[6] and they are outlined in Figure 2. In the first proposed mechanism D-Glu binds in

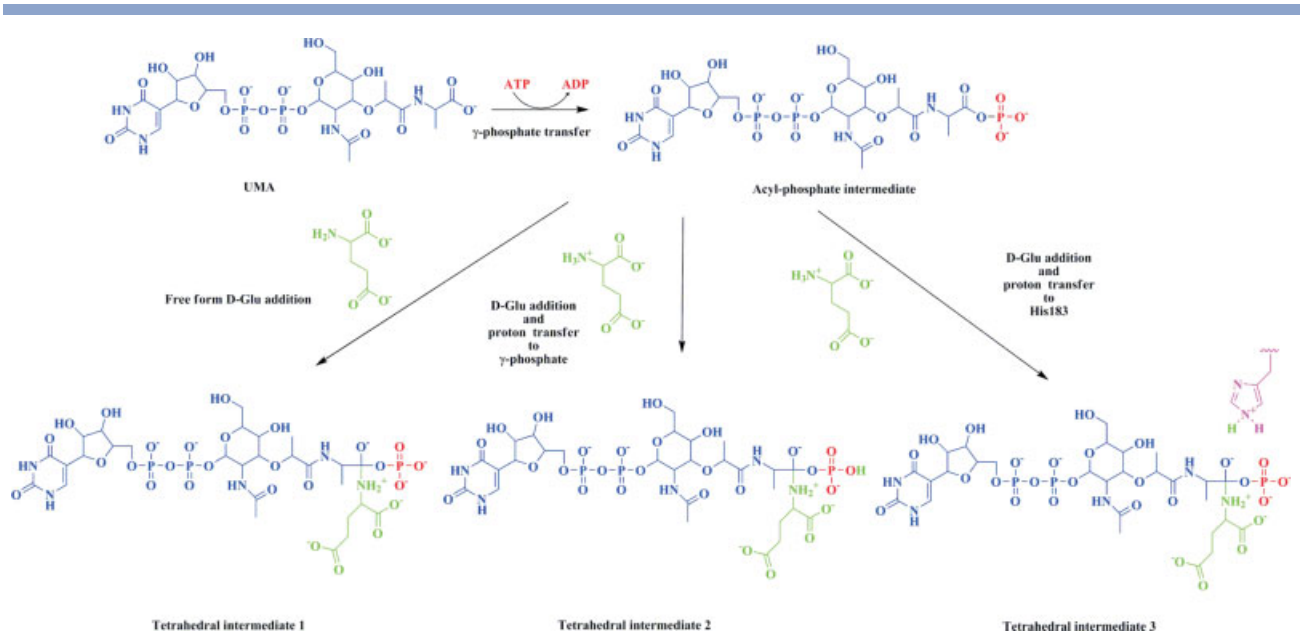

Figure 2

The proposed sequential reaction mechanism of the MurD reaction affording the tetrahedral intermediate.[6–8] The first stage involves the γ-phosphate transfer from ATP to UMA to yield the acyl-phosphate intermediate. Subsequently, the nucleophilic attack of the D-Glu moiety results in a tetrahedral intermediate formation. Three possible mechanisms of this catalytic step are depicted. [Color figure can be viewed in the online issue, which is available at www.interscience.wiley.com.]

its free base form and is therefore deprotonated before entering the amide-forming reaction, yielding the tetrahedral intermediate **1**. An analysis of the possible proton acceptors located in the vicinity of the MurD reaction site revealed ATP γ-phosphate and His183 (located at 4.2 Å away form UMA substrate) as possible proton acceptors. Two additional mechanisms of tetrahedral intermediate formation were hypothesized where D-Glu participates in the reaction in its protonated form.[6] One possibility suggests that ATP γ-phosphate acts as a catalytic base that accepts the D-Glu proton, yielding the tetrahedral intermediate **2**. His183, though not mentioned explicitly in the context of C—N bond formation, but as a potential proton acceptor for the second proton transfer, could equally be considered providing the tetrahedral intermediate **3**. In the final step of this complex enzymatic reaction, the dissociation of the phosphate group from the tetrahedral intermediate, together with another base-assisted proton transfer, takes place, which results in the final MurD product UMAG.

Structural and site-directed mutagenesis experiments provided a considerable amount of data regarding the MurD enzyme. Because of the undisputable attraction of this enzyme as a potential drug target several inhibitors of MurD were designed.[19] One of the first published approaches which took the enzymatic process into account was a design of enzyme inhibitors based on a proposed structure of the tetrahedral intermediate. It was speculated that a placement of phosphonic acid between L-Ala and D-Glu would yield a structure closely mimicking the original tetrahedral species or even its transition state. The binding constant of the phosphinate inhibitor comprising L-Ala, D-Glu, phosphinate moiety, and uridine diphosphate was determined to be as low as 170 nM.[20] In addition, in the case of a closely functionally related enzyme D-Ala-D-Ala ligase an inhibitor with this moiety has a decomplexation half-life of 17 days, which renders such noncovalent inhibitor effectively irreversibly bound to the enzyme.[21] Thus, we reasoned that initial model for our end point of the reaction—tetrahedral intermediate—should closely mimic the structure of this inhibitor. Following the initial success of this approach several low-molecular-weight analogues of the tetrahedral transition state were published, mostly classified as phosphinate and sulphone amide derivatives of D-Glutamic acid.[22,23] Recently, the first crystal structures of MurD bound with *N*-sulfonamide D- (and L-) Glu inhibitors revealed the binding mode of this class of inhibitors.[24]

Molecular modeling of covalent bond making and bond breaking processes, as is the case in the MurD enzymatic reaction, requires the application of quantum-chemical methodology.[25] Because of vast computational requirements, hybrid quantum mechanical/molecular mechanical (QM/MM) methods were introduced that enable the study of such processes within reasonable time scales.[26] The standard approach involves a division of

biomolecular system into a smaller (reaction) region which is treated with a selected QM level of theory while the remaining larger part is described with a classical molecular mechanics force field.[27,28] As a boundary between the QM an MM region in enzyme reactions is likely to cross at a covalent bond, electron density between the regions must be carefully treated to avoid unphysical results. The most popular link atom method[28] involves a saturation of an open QM valence with an extra atom (mostly hydrogen); however several other methods have also been developed.[29]

A significant advantage of *in silico* studies of enzymatic reactions is the possibility to explore and evaluate several possible mechanisms that could be derived from experimental observations. Determining the course of events in the transformation from the starting (reactants) to its final (products) system configuration is a task solved by reaction pathway methods.[30] Pathway determination, which is based on an analytic Hessian computation of potential energy and is used for small molecules, is prohibitively expensive, so for large macromolecular systems other methods must be exploited such as, for example, the restrained coordinate driving (RCD) method[30] where the reaction is forced to occur by restraining the system to a predefined chemically relevant reaction coordinate. This latter method suffers from hysteresis problems due to the severe constraints imposed on the reaction coordinate.[31] A recently proposed method to determine reaction pathways avoiding this problem is QM/MM Replica Path Method (RPATh),[31–34] an extension of the self-penalty walk method by Elber and co-workers,[35,36] which involves a simultaneous optimization of a series of geometries of the reacting system, corresponds to a series of points along the reaction pathway (described in detail in Methods section). Thus the approximate minimum energy pathway (MEP) is generated, having a benefit over the reaction coordinate driving approach because it eliminates the bias in choosing the reaction coordinate. The RPATh method uses root mean square distance (RMS) changes to define the distance between two points on the approximate MEP. This allows the "global pathway" motion to define a reaction path rather than relying on a combination of distances, as in the more frequently used RCD method.[32]

In this work, as part of our ongoing investigations of the MurD enzyme as an attractive antibacterial target, we present results of hybrid QM/MM studies of a tetrahedral intermediate formation an approved drug design starting point. Three reaction pathways—**RPATh 1-3** (see Fig. 2) between pairs of optimized starting structures and tetrahedral intermediates were mapped by QM/MM replica path method and thus enabling an assessment of the reaction pathways and offering direct comparison with the Mur ligase familiy sequential kinetic mechanism[7,8] and available MurD structural data.[6]

METHODS AND COMPUTATIONAL STRATEGIES

Preparation of the enzyme-substrate complex—starting structures

In the initial preparation step, the starting structures **I–III** with identical system configurations but different QM regions of the MurD system and three possible configurations of the tetrahedral intermediate **1–3,** were determined to inspect the geometry and energy difference between the species. Coordinates of the experimentally determined MurD structures were retrieved from the Protein Data Bank (PDB code: 2UAG).[6] The 2UAG crystal structure was chosen since it provides experimental coordinates of both magnesium ions that were shown to be essential for Mur ligase enzymatic activity.[37] Hybrid QM/MM calculations were carried out to study the structure and energy profile of the MurD reaction using the CHARMM molecular mechanics force field[38] interfaced with *ab initio* quantum chemistry package GAMESS.[39] The defined quantum regions 1–3 were treated with the B3LYP density functional level of theory (DFT)[40] in conjunction with the 6-31G(d) basis set. CHARMM parameter and topology files (version 27) for proteins and nucleic acids were utilized to specify force field parameters describing the protein, classical parts of the UMA substrate, ATP, and carbamylated Lys198 residue.[41–44] In the 2UAG structure, amino acid residues 220–224 and 242–244 were not visible in the experimental electron density map and were constructed using CHARMM. All calculations were performed on Beowulf-type CROW clusters[45] at the National Institute of Chemistry in Ljubljana, Slovenia.

Hydrogen atoms were added using the CHARMM HBUILD routine. To complete the MurD system two additions to available experimental data had to be introduced. The original 2UAG structure contains ADP as a ligand, therefore CHARMM building capabilities were used to construct the third γ-phosphate group as suggested by Dideberg *et al.*, positioning first phosphate oxygen as a ligand for the Mg^{2+} located in the pocket between UMA and ADP and the second coordinated with N^{ζ} of Lys115 to make a fully functional ATP molecule.[6] D-glutamate representing the condensing amino acid in the MurD reaction was generated using CHARMM and positioned in the D-Glu binding site identified in the product UMAG 4UAG crystal structure. The γ-carboxylic group was placed within a hydrogen bonding distance of Phe422 and Ser415, and the α-carboxylic group interacted with Thr321 and Lys348.[6] However, D-Glutamate was still positioned out of the covalent bonding range of UMA (distance between the reacting atoms being ~3.2 Å). This configuration formed the starting structures **II** and **III** while the starting structure **I** was created by deletion of one of the D-Glu amide

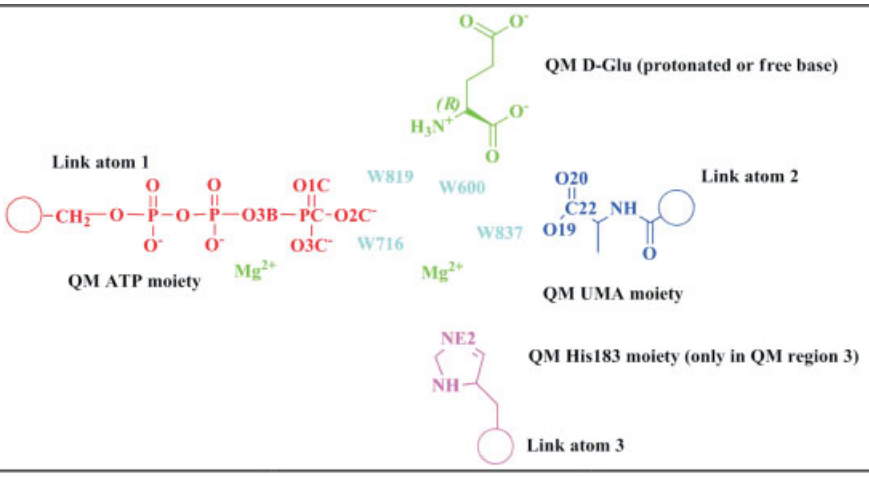

	QM atoms	Reaction path
QM region 1	63	(1)
QM region 2	64	(2)
QM region 3	72	(3)

Figure 3

QM regions of the MurD system with defined important atom indexes used in this study. [Color figure can be viewed in the online issue, which is available at www.interscience.wiley.com.]

hydrogens. All crystal waters provided in the 2UAG structure were conserved during QM/MM simulations and the MurD starting systems were further hydrated by immersion into a cubic box (100 Å × 100 Å × 100 Å) of water molecules.[46] After hydration, water molecules located more than 4 Å away from the enzyme were removed, resulting in macromolecular systems composed of either 16,075 or 16,074 atoms. These two systems were initially minimized using modified Adopted Basis Newton-Raphson (ABNR) method[38] until the root-mean-squared gradient (GRMS) was consistently less than 0.001 kcal/mol/Å. Starting structures **I–III** that represented configurations of MurD prior to enzyme reaction were derived from these initial structures by a subsequent QM/MM minimization, each structure with its own QM region as described below, using a modified ABNR method until the root-mean-squared gradient (GRMS) was consistently less than 0.001 kcal/mol/Å. The MurD including free base D-Glu with QM region **1** (starting structure **I**) and two protonated D-Glu systems were minimized with QM region **2** (starting structure **II**) and QM section **3** (starting structure **III**) for the reaction path **RPATh 3**.

Three QM regions which were used in QM/MM replica path calculations as well as in QM/MM geometrical optimizations of starting structures and tetrahedral intermediates of MurD are depicted in Figure 3 together with atom indexes used in presenting the geometrical parameters of the reaction mechanism. They all consisted of three phosphate moieties of ATP sliced at the C4′—C5′ bond in the ATP ribose subunit, two magnesium ions, D-Glu amino acid (free or protonated form), four crystal waters: W600, W716, W819, and W837 located in the reacting area and additionally the side chain of His183 in QM region **3** where protein transfer from D-Glu to His183 was studied. Empty valences of QM UMA and QM ATP (and QM His183) moieties were filled with standard link-atom hydrogens.[28] Other atoms outside the QM region were treated with the CHARMM empirical force field.

Tetrahedral intermediates investigations

The minimized geometries of the starting structures **I–III** served as a starting point for the determination of tetrahedral intermediate structures. As two covalent bonds are required to be formed to yield the tetrahedral intermediate, its geometry was calculated in two steps, applying the CHARMM restrain distance (RESD) methodology.[30] In our case, the simplest form of this general approach was used by adding a restraint to the CHARMM potential energy function prescribing the movement along the chemically relevant reaction coordinate and forcing the formation of the desired chemical bond[30]:

$$E_{\mathrm{RESD}} = \frac{k_j}{2}\left(d_0 - d_{\mathrm{eq}}\right)^2 \qquad (1)$$

where k_j is the applied force constant, d_0 selected interatomic distance between pair of selected atoms, and d_{eq} is the target interatomic distance.

In the first step of the procedure, the distance between the PC γ-phosphorus atom and the O19 UMA carboxylate oxygen was restrained to 1.6 Å in 100 steps of RESD QM/MM minimization and then minimized with the previous constraint removed. The value of k_j was set to 100.0 kcal/mol/Å^2 and no weighting factor was introduced. A stable covalent bond distance between the γ-phosphorus atom of ATP and the UMA carboxylate oxygen after the restraint term release was taken as a benchmark for the validation of a stable acyl-phosphate intermediate.

In the second step, the obtained acyl-phosphate intermediates and structure of the phosphinate inhibitor[20] were used to generate the tetrahedral intermediate structures **1–3**. The first tetrahedral intermediate configuration—tetrahedral intermediate **1**—was determined by restraining the amine nitrogen of the free base D-Glu moiety to a covalent distance (1.5 Å) of the C22 UMA terminal carbonyl atom. The CHARMM RESD methodology was used (k_j = 100.0 kcal/mol/Å^2 and no weighting factor) in 100 QM/MM minimization steps, which was followed by an unrestrained minimization utilizing QM region **1**. The remaining two tetrahedral intermediates **2** and **3** with protonated D-Glu were generated in a similar fashion using the same distance constraint for the C—N bond formation and adding an additional distance constraint with k_j = 100.0 kcal/mol/Å^2 to drive the proton from D-Glu to either the O3 oxygen of γ-phosphate using QM region **2** or to the NE2 nitrogen of His183 applying QM region **3**. All tetrahedral intermediates **1–3** were subsequently QM/MM minimized without constraints until the root-mean-squared gradient (GRMS) was less than 0.0001 kcal/mol/Å.

Generation of reaction pathways between the starting and tetrahedral intermediate structures by the QM/MM replica path method

Three reaction pathways starting from corresponding QM/MM geometrically optimized starting and tetrahedral reaction intermediates **1–3** were generated by the QM/MM replica path method (RPATh).[31] Simultaneous optimization of a series of geometries (replicas) of the reacting system corresponding to a series of points along the reaction pathway was performed.[31] The target function for the combined minimization involves the standard sum of the configurational energies, together with a series of penalty functions that ensure that the generated replicas represent the reaction pathway. A force constant is used to restrain the distances between adjacent pathway points, ensuring that the generated pathway is smooth and evenly spaced [Eq. (2)]:

$$E_{\mathrm{RMS}} = \sum_{i-1}^{\mathrm{NREP}-1} \frac{1}{2} K_{\mathrm{rms}} (\mathrm{rms}(i, i+1) - \langle \mathrm{rms} \rangle)^2 \qquad (2)$$

where NREP is the number of generated replicas along the pathway, rms(i,i+1) is the best fit RMS value [Eq. (3)] between successive replicas, and ⟨rms⟩ is the average RMS value [Eq. (4)]:

$$\mathrm{rms}(i, i+1) = \sqrt{\frac{\sum_{j=1}^{\mathrm{NATOM}} w_j \left[(x_j^{(i)} - x_j^{(i+1)})^2 + (y_j^{(i)} - y_j^{(i+1)})^2 + (z_j^{(i)} - z_j^{(i+1)})^2 \right]}{\sum_{j=1}^{\mathrm{NATOM}} w_j}} \qquad (3)$$

and

$$\langle \mathrm{rms} \rangle = \frac{\sum_{i=1}^{\mathrm{NREP}-1} \mathrm{rms}(i, i+1)}{\mathrm{NREP}} \qquad (4)$$

$$w_j = w(\mathrm{factor})_j x(\mathrm{atomic\ mass})_j \qquad (5)$$

where $x_j^{(i)}$ represents the x coordinate of atom j in replica i and $x_j^{(i+1)}$ the x coordinate of atom j in replica i + *1* and w_i is atom-mass based weighting factor in Eq. (5) that ensures that atoms of interest are weighted more than the surrounding bulk, thus reducing the overestimation of those atoms that are not significantly involved in the reaction.

A second force constant is used in a replica path penalty term to restrain the angle between an adjacent and the next adjacent pathway points (i, $i \pm 1$, $i \pm 2$) using the law of cosines, thus avoiding paths that double back on themselves [Eqs. (6)–(8)].

$$E_{\mathrm{angle}} = \sum_{i=1}^{NREP-2} \frac{1}{2} K_{\mathrm{angle}} (\mathrm{COSMAX} - \cos(\theta)_i)^2 \qquad \mathrm{COSMAX} > \cos(\theta)_i \qquad (6)$$

$$E_{\mathrm{angle}} = 0 \qquad \mathrm{COSMAX} \leq \cos(\theta)_i \qquad (7)$$

$$\cos\theta = \frac{\mathrm{rms}(i, i+2)^2 - \mathrm{rms}(i, i+1)^2 - \mathrm{rms}(i+1, i+2)^2}{2\mathrm{rms}(i, i+1)\mathrm{rms}(i+1, i+2)} \qquad (8)$$

In the replica path procedure, starting replica geometries must be generated before geometrical optimization

of the reaction path can commence, either by a simple interpolation of Cartesian coordinates or more a sophisticated approach such as internal coordinate manipulation.[31] Additionally, the highly parallel nature of the RPATh method makes it attractive for computationally demanding QM/MM optimization algorithms since each generated replica can be allocated to a different set of processors within a cluster and communication among the processor subsets is necessary only when a QM step is completed.[31]

The 15 initial replicas for each of the investigated reaction pathways (**RPATh 1–3**) were generated by linearly interpolating the coordinates between all atoms of the QM/MM geometrically optimized starting structures **I–III** and the corresponding tetrahedral intermediates **1–3**. The number of replicas was chosen on the basis of previous benchmark calculations on chorismate mutase,[31–33] as well as calculated RMS difference between the initial RESD generated and corresponding replica structures (available in the supplementary material). These values, which in all three cases are within the range of 0.5 Å provides the average RMS distance of about 0.05 Å between points on each RPATh. Geometry optimizations of replica paths **RPATh 1–3** were performed using the ABNR method which was extensively tested previously.[32] Parameters included in the QM/MM replica path penalty terms were set to the following values: K_{rms} = 5000.0 kcal/mol/Å,^{2} K_{angle} = 100.0 kcal/mol/Å, and COSMAX = 0.95 radian. Only the QM region was weighted in the replica path RMS calculation to avoid overestimating the contributions of atoms not significantly involved in the reaction. Reaction pathways were minimized until the total pathway root-mean-squared gradient (GRMS) was consistently less than 0.01 kcal/mol/Å and total pathway energy change was less than 1.0 kcal/mol for at least 30 consecutive steps. Each calculation was conducted on a set of 60 CPU units (4 CPU/replica) within the CROW cluster. Results of QM/MM simulations were visualized using the VMD software[47] and energy diagrams were created using the Gnuplot program.[48]

RESULTS AND DISCUSSION

Investigation of the starting structures

We have used available experimental data for the starting structures from protein crystallography,[6] biochemical proof of the acyl-phosphate intermediate existence,[9,10] and the structure of the irreversible noncovalent inhibitor with phosphinate moiety,[20] anchored in the enzyme active site, as determined by crystal structure of similar sulfonamide inhibitors in complex with MurD ligase.[24] Thus three starting points on the MEP: starting structure, acyl-phosphate intermediate, and tetrahedral intermediate are supported by some key structural data, allowing for a reasonable comparison study of the three possible pathways proposed by Dideberg and coworkers.[6]

The prepared MurD starting structures were first subjected to a classical energy minimization. The carboxylic groups of the D-Glu moiety were positioned within a hydrogen bond distance observed for the product UMAG in the 4UAG structure.[6] Subsequent QM/MM minimization of the MurD systems with three selected QM regions yielded the structures, which should be the closest approximation of the MurD enzyme prior to enzymatic reaction. The important geometric information about the starting structures **I–III** is collected in Table I and in Figure 4 the superimposed structures of all reacting partners together with QM treated crystal waters as well as magnesium ions and link atoms are depicted.

The distance between reacting partners UMA and ATP γ-phosphate was 0.15 Å longer in the starting structure **I** due to the deletion of a hydrogen atom affording free base D-Glu. The condensing amino acid D-Glu was located far from the UMA covalent bonding distance (3 Å). No major difference could be observed for the distance between His183 and D-Glu. The overall uniformity of the starting conformations can be observed in Figure 4.

In Table I the distances between D-Glu moiety and enzyme MurD atoms are collected. Distances were measured following the interactions of the product UMAG in

Table I
Values of Important Bond Lengths and Interaction Distances in Starting Structures I–III

Bond distance	Starting structure **I** (Å)	Starting structure **II** (Å)	Starting structure **III** (Å)
D-Glu (OE1):Ser415 (N)	4.22	3.71	3.70
D-Glu (OE1):Ser415 (OG)	4.37	4.28	4.28
D-Glu (OE2):Phe422 (N)	4.82	4.78	4.77
D-Glu (OT1):Lys348 (NZ)	3.98	3.81	3.82
D-Glu (OT2):Thr 321 (OG1)	4.25	3.75	3.75
D-Glu (N):His183 (NE2)	5.00	4.87	5.05
UMA (O19):γ-phosphate (PC)	2.92	2.77	2.77
UMA (C22):D-Glu (N)	3.13	3.08	3.08
Phe422 (O):Lys319 (NZ)	2.73	2.74	2.75

Column 2: Starting structure **I** (deprotonated D-Glu moiety), Column 3: Starting structure **II** (protonated D-Glu moiety, QM region 2), Column 4: Starting structure **III** (protonated D-Glu moiety, QM region 3).

the 4UAG crystal structure.[6] A careful analysis showed that during the minimization procedure, a slight reorganization of the hydrogen bonds occurred for D-Glu interactions. In this new pattern the OT2 oxygen of the D-Glu α-carboxylate interacts with Lys348 (distances around 2.6 Å). Additionally, the backbone nitrogen N and the side chain oxygen (OG) of Ser415 (distances around 3.5 Å and 2.60 Å) interacts with the γ-carboxylate oxygen OE2 that interacts with Phe422 in original the 4UAG.

The most noticeable difference was a complete loss of the hydrogen bond between the γ-carboxylic group and backbone nitrogen of Phe422. This residue is located on the protein loop (residues 419–425) between the β20 and α16 helix.[6] It was observed that in the 2UAG structure this loop did not adopt a β helical conformation, which was observed in the other MurD structures.[6] Its position in 2UAG and 4UAG as well as in the fully QM/MM optimized starting structure **I** is depicted in Figure 5 together with the ATP molecule shown for comparison. When analyzing the available MurD crystal structures Dideberg *et al.* established that this loop conformational change can be attributed to a repulsive interaction between the side chain of Lys319 and a magnesium ion located between β- and γ-phosphate of ATP in a "classical magnesium binding site" of 2UAG.[6] In all other crystal structures the side chain of Lys319 extended down to the close vicinity of the γ-phosphate also illustrated in Figure 5 for the 4UAG structure.[6] Application of distance restrained-minimization that forced the γ-carboxylate oxygen of D-Glu within a hydrogen binding distance of Phe422, led to the reconstitution of the initial state immediately after the constraint release. The presence of two magnesium ions has been experimentally observed in the MurC ligase (PDB code: 1P3D) crystal structure where the γ-phosphate of non-hydrolysable ATP analogue AMPPNP was found to be constrained between two magnesium ions. This finding further supported the presence of two magnesium ions during catalysis for the Mur ligase family.[49]

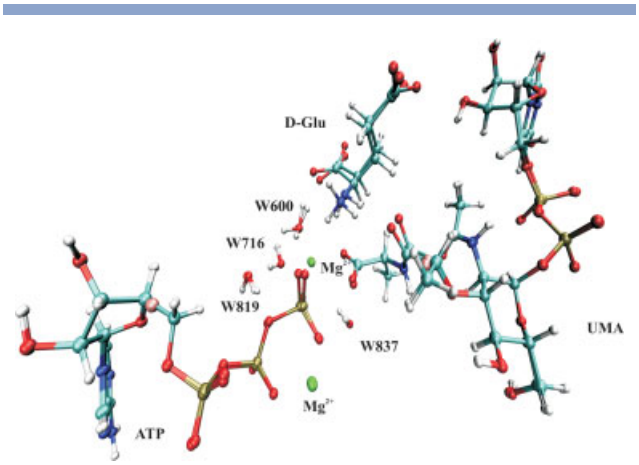

Figure 4

Superimposed geometries of the reacting species (UMA, ATP, D-Glu), together with QM treated waters and magnesium ions of the QM/MM optimized starting structures **I–III**. Link atoms between ATP and UMA are depicted in pink. [Color figure can be viewed in the online issue, which is available at www.interscience.wiley.com.]

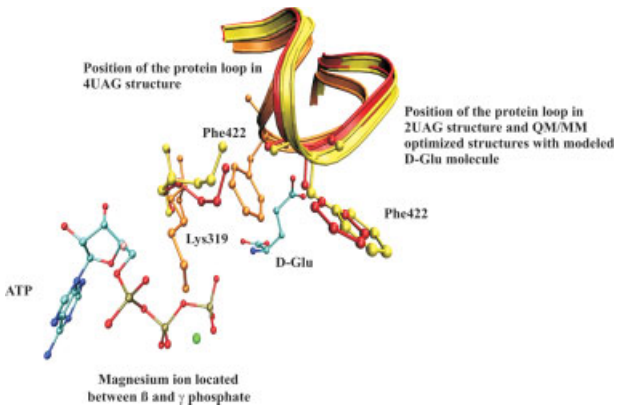

Figure 5

Observed positions of the Lys319 and Phe422 residues and the protein loop reorganization in different MurD systems. In orange the conformation of the protein loop in 4UAG[6] (identical to 3UAG) is shown, in red and yellow the positions of 2UAG[6] and QM/MM fully minimized starting structure **I** are depicted, respectively. [Color figure can be viewed in the online issue, which is available at www.interscience.wiley.com.]

To investigate the loop movement even further, the Lys319 residue and loop residues 419–425 as found in 4UAG were included in our investigated structure. This structural modification was quite straightforward, as experimental coordinates for the backbone atoms of the 2UAG and 4UAG structures superimposed with a RMS value of 0.55 Å (all backbone atoms). The structure was then relaxed by a minimization procedure. Subsequent distance-restrained minimizations were performed in a similar fashion as described. The presence of a magnesium ion between β and γ-ATP phosphate induced movement of a positively charged side chain of Lys319 away from the original 4UAG position and simultaneously inducing a loop conformational change towards the conformation found in the 2UAG structure and losing the hydrogen-bond interaction with γ-D-Glu carboxylate oxygen OE2. Our results suggest that the presence of the catalytic magnesium ion between β- and γ-ATP phosphate does not allow Phe422 to adopt the helical conformation.

Structures of the tetrahedral reaction intermediate

Our two-step computational procedure leading to tetrahedral intermediate structures **1–3** using the RESD methodology showed that in the first step of the proce-

Table II
Values of Important Bond Lengths and Interactions Distances for Tetrahedral Intermediate Structures 1–3

Bond distance	Tetrahedral intermediate **1** (Å)	Tetrahedral intermediate **2** (Å)	Tetrahedral intermediate **3** (Å)
D-Glu (OE1):Ser415 (N)	3.79	3.67	3.57
D-Glu (OE1):Ser415 (OG)	4.36	4.31	4.29
D-Glu (OE2):Phe422 (N)	4.95	4.93	5.02
D-Glu (OT1):Lys348 (NZ)	3.99	3.66	3.07
D-Glu (OT2):Thr 321 (OG1)	3.27	2.91	3.56
D-Glu (N):His183 (NE2)	4.54	4.53	5.30
UMA (O19):γ-phosphate (PC)	1.68	1.62	1.69
UMA (C22):D-Glu (N)	1.65	1.57	1.64
Phe422 (O):Lys319 (NZ)	2.75	2.75	2.83

Column 2: Tetrahedral intermediate **1** (deprotonated D-Glu moiety), Column 3: Tetrahedral intermediate **2** (protonated D-Glu moiety, QM region 2), Column 4: Tetrahedral intermediate **3** (protonated D-Glu moiety, QM region 3).

dure, the inclusion of crystal waters W600, W716, W819, and W837, enveloped around the reaction area between UMA and ATP in the QM region, was required to yield a stabile acyl-phosphate species. Distances between reacting atoms phosphorus PC and oxygen O19 in the obtained acyl-phosphate structures after the distance constraint release stabilized at 1.8 Å. Our results indicate that beside the magnesium ions and Lys115, which facilitate the γ-phosphate transfer,[6] water molecules apparently play an important role in the stabilization of the formed intermediate. Structure comparisons and superimposed geometries of the QM/MM optimized acyl-phosphate intermediates are provided in the supplementary material.

The final optimized geometries of the tetrahedral reaction intermediates **1–3** are collected in Table II and in Figure 6 the superimposed tetrahedral structures together with QM treated crystal waters, magnesium ions, and link atoms are depicted. The newly formed C—N bond stabilized at 1.6 Å. The length of the C—N bond was longer compared to a normal peptide bond. This observation was anticipated due to the presence of a phosphate group adjacent to the UMA C22 atom and an

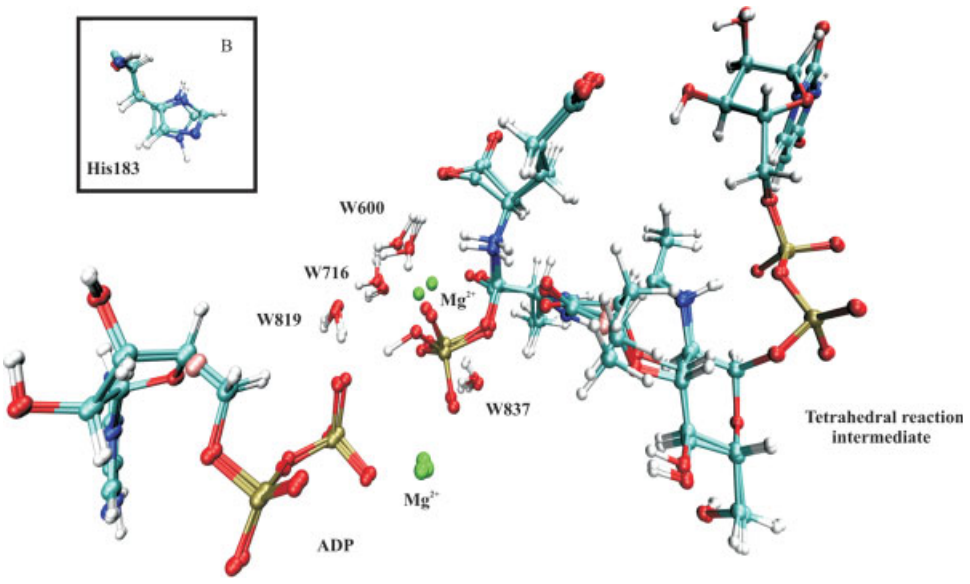

Figure 6
Superimposed geometries of the optimized tetrahedral reaction intermediates **1–3**, together with ADP, QM treated waters, and magnesium ions. Link atoms between ATP and UMA are depicted in pink. **B:** Positions of His183 in superimposed tetrahedral reaction intermediates **1–3**. [Color figure can be viewed in the online issue, which is available at www.interscience.wiley.com.]

additional proton on the D-Glu nitrogen atom. Previously formed covalent bond between γ-phosphate residue and UMA changed from 1.8 Å in the acyl-phosphate intermediate to 1.6 Å.

Monitored hydrogen bonds between tetrahedral intermediates **1–3** and MurD enzyme remained mostly identical as observed in starting structures **1–3** (Table II). Noticeable differences occurred in the interaction between the backbone nitrogen of Ser415 in tetrahedral intermediate **1** where this distance was shortened to 3.79 Å. Also more favorable was the distance between the D-Glu moiety and the charged nitrogen of Lys319 for the tetrahedral intermediate **3**. Interestingly, in tetrahedral intermediates **1** and **2**, hydrogen bonds with Thr321 not detected in the starting structures were observed.

Energy differences were calculated between pairs of corresponding tetrahedral intermediates **1–3** and the starting structures **I–III**. The first investigated pair of structures with deprotonated D-Glu acquired an energy difference of 0.8 kcal/mol, indicating a modest endothermic character of this part of the MurD reaction. The second pair: tetrahedral intermediate **2** with a proton on γ-phosphate and corresponding starting structure displayed similar difference of 0.26 kcal/mol. In the third pair, with a proton located on His183, a highly endothermic nature of the reaction was indicated since the energy difference between the structures was 14.8 kcal/mol. The obtained results were in accordance with the speculation of a high-energy tetrahedral intermediate, which, after the dissociation of the phosphate group, yields the final product UMAG.[6]

Since different QM regions were used in the minimization procedure only corresponding pairs could be directly compared. To probe the relative transferability, the starting structure **II** and tetrahedral intermediate **2** were fully re-optimized with a QM region **3**. The obtained energy difference was adequately comparable with the difference obtained with a smaller QM region.

QM/MM replica path optimized reaction pathways

QM/MM optimized pairs of starting structures **I–III** and tetrahedral intermediates **1–3** represented the boundary structures for the generation of reaction pathways (**RPATh**) **1–3**. We were especially interested if the generated reaction pathways could provide information about the course of events during the conversion of starting configurations to tetrahedral intermediates as the postulated kinetic mechanism established by experimental studies on other Mur ligases of this enzyme family suggested a sequential reaction mechanism commencing with the formation of acyl-phosphate and a subsequent reaction with D-Glu.[7,8] Unlike traditional scan calculations commonly used in modeling of enzyme mechanisms and which impose severe constraints in the reaction coordinate, the QM/MM replica path method allows the concerted movement of all atoms not predetermining the movement along the reaction coordinate.[31] This was a particularly favorable feature of the RPATh method used in our study since the order in which substrates enter the reaction was also investigated.

We have generated the geometries by using RESD procedure in three key points of the MurD reaction based on the available experimental data. The replica pathways were started without any bias towards the midway point (acyl-phosphate formation) and were checked against RESD-generated geometries. It was gratifying to observe that the comparison of the two sets of structures (Table II(S) of the supplementary material) gives RMS values that are smaller than 0.4 Å. This excellent match between the RESD generated geometries at the midway point of the reaction (acyl-phosphate structures) and the RPATh generated geometries (the RPATh approach uses only the starting and final geometry of the reactants and products, respectively) shows that the replica pathways follow the course of the reaction as we hypothesized at the outset of the simulation.

All atoms of the MurD systems were replicated by making a linear interpolation of coordinates between pairs of boundary structures resulting in three systems of 15 replicas. The full replication of the MurD system was possible because only minor conformational changes were observed when comparing pairs of boundary structures by visual inspection and RMS calculations (available in the supplementary material). In particular, an absence of otherwise frequently occurring rotations of water molecules between boundary structures on the MurD molecular surface allowed that the examined potential energy was a meaningful quantity even with full replication.[33] Additionally, the problems associated with "average structure" produced for the non-replicated part were no longer present, which considerably improved the quality of the generated pathway. Animations of QM/MM replica path optimized reaction pathway **1–3** (available in the supplementary material) serve for a better visualization of the results discussed bellow.

Replica path 1

Replica path **1** (**RPATh 1**) described the reaction path between starting structure **I** and tetrahedral intermediate **1** outlining the mechanism in which D-Glu enters the reaction in its free base form. In Figure 7 the **RPATh 1** energy diagram is presented, describing the energetics along the reaction coordinate determined by the replica path method. The reacting order of the compounds as determined by replica path calculations agreed with the proposed kinetic mechanism of the Mur family.[7,8] Between replicas 1–8 a γ-phosphate transfer occurred, yielding the acyl-phosphate intermediate and stabilizing the newly formed bond at 1.8 Å. The distances between

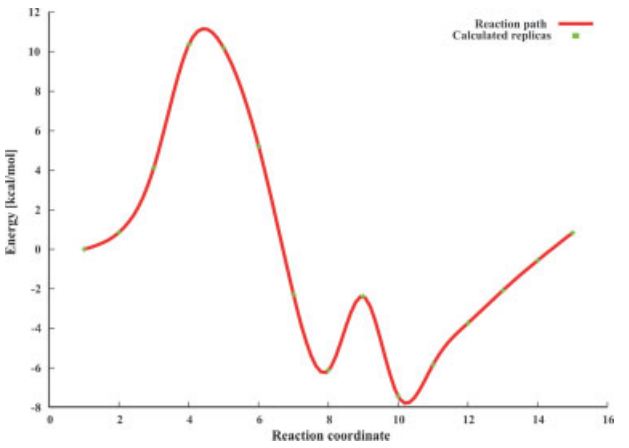

Figure 7

Energy diagram for the QM/MM optimized reaction pathway **RPATh 1** describing energetics along the reaction coordinate during the transformation of starting structure **I** to tetrahedral reaction intermediate **1**. [Color figure can be viewed in the online issue, which is available at www.interscience.wiley.com.]

reacting atoms can be observed in Table III. A careful inspection of the obtained geometries revealed that γ-phosphate transfer proceeded through a bi-pyramidal transition state with an energy barrier of ∼10 kcal/mol. Replica 4 could be considered as the closest approximation of the transition state structure. The course of phosphate transfer was well in accordance with the S_N2 reaction mechanism proposed by the structural studies.[6] The final energy of the acyl-phosphate intermediate was located 6 kcal/mol lower compared to the starting configuration.

Notably, no changes were observed for the distance between D-Glu and UMA during the acyl-phosphate intermediate formation as the C—N distance remained unchanged between 3.1 and 3.2 Å. This observation is important as kinetics studies also determined the binding order of the reacting compounds, starting with the binding of ATP, followed by UMA and lastly D-Glu binding.[7,8] The bonding process itself was not possible to model simultaneously with the reaction and we are aware that in this respect, the constructed starting structure and the model itself represent a simplification of the MurD state during the reaction. However, the order of the ligands entering the reaction obtained by the QM/MM replica path procedure is clearly in agreement with the experiment.

In the next phase of the reaction mechanism **1** D-Glu amine hydrogens underwent pyramidal inversion, positioning the D-Glu nitrogen lone pair for the subsequent C—N bond formation. This is visible in Figure 7 as a second transition state represented by replica 9 in which an energy rise of 4 kcal/mol compared with the acyl-phosphate was observed. In replica 10 an energy drop was observed due to a more favorable geometry of D-Glu for the C—N bond formation but nevertheless the distance 2.8 Å between the species was still far from the covalent binding distance. In the following replicas 11–15 D-Glu moved within the covalent binding distance. Surprisingly, we observed that the formation of the C—N bond was coupled to an unexpected energy rise in yielding the final tetrahedral formation. Several reasons could be speculated for this unanticipated observation. Since the precise geometry of the tetrahedral intermediate is unknown and largely derived from the identified transition state inhibitors,[20] it is possible that some additional event must occur simultaneously with the C—N bond formation leading to a tetrahedral structure. For example, a transfer of a second D-Glu proton during the C—N bond formation could provide an explanation. Another possible option is that in the case of the deprotonated D-Glu, a water molecule hindered the C—N formation. Since the D-Glu moiety was inserted by modeling into the starting 2UAG crystal structure the positions of water molecules in the hydration shell may have been insufficiently treated by QM/MM minimization.

Replica path 2

Calculated replica path **2** (**RPATh 2**) corresponded to the reaction mechanism where deprotonation of D-Glu during tetrahedral intermediate **II** formation was assisted by the γ-ATP phosphate. In Figure 8 an energy reaction profile as obtained from the QM/MM replica path calcu-

Table III

Variation of Important Bond Lengths (in Å) Along the Reaction Pathway Versus Replica Step Number in the Optimized QM/MM Replica Path RPATh 1

Reaction path step	PC (ATP)-O19 (UMA) (Å)	PC (ATP)-O3B (ATP) (Å)	N (D-Glu)-C22 (UMA) (Å)
1	2.92	1.75	3.13
2	2.81	1.76	3.14
3	2.62	1.86	3.16
4	2.38	2.07	3.19
5	2.11	2.39	3.22
6	1.92	2.69	3.25
7	1.83	2.93	3.24
8	1.79	3.14	3.16
9	1.77	3.32	2.97
10	1.75	3.48	2.79
11	1.74	3.62	2.58
12	1.73	3.73	2.34
13	1.71	3.78	2.06
14	1.69	3.78	1.80
15	1.68	3.74	1.65

Column 2: distance between the reacting γ-phosphate atom and the UMA terminal oxygen, Column 3: distance between the bond-breaking γ-phosphate and β-phosphate of ATP, Column 4: distance between the reacting terminal carboxylic UMA carbon and the amine nitrogen of D-Glu.

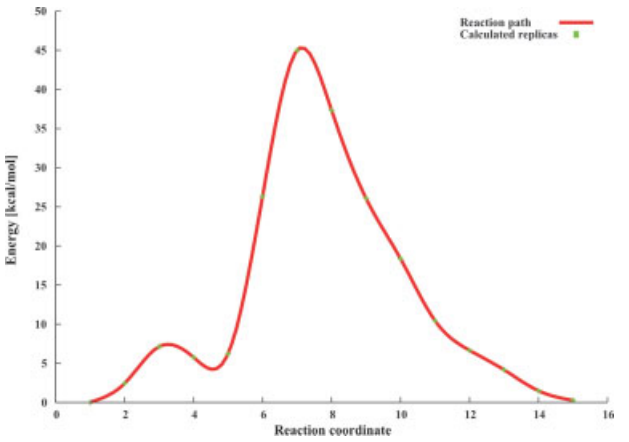

Figure 8

Energy diagram for the QM/MM optimized Reaction pathway **RPATh 2** describing energetics along the reaction coordinate during the transformation of starting structure **II** to tetrahedral reaction intermediate **2**. [Color figure can be viewed in the online issue, which is available at www.interscience.wiley.com.]

lations is outlined. In the initial reaction pathway replicas the PC γ-phosphorus atom moved within a covalent binding distance of UMA carboxylate oxygen O19 (Table IV). The distance between carbonyl oxygen C22 and the D-Glu amine nitrogen, however, remained almost unchanged during the acyl-phosphate intermediate formation (varying between 3.2 and 2.9 Å). This observation again is well corroborated with a sequential reaction mechanism.[7,8]

Detailed energetic analysis of the first part of reaction pathway **RPATh 2** revealed that during the acyl-phosphate formation an energy barrier of ~7 kcal/mol had to be crossed. Inspection of the geometries allocated to replicas 2–4 revealed that the γ-phosphate transfer here again proceeded through a bi-pyramidal transition state. Here replica 3 represented the approximate geometry of the bi-pyramidal transition state. After inversion of the γ-phosphate oxygen atoms, the newly formed P—O bond stabilized at 1.8 Å in replica 6. This result is again in agreement with the proposed S_N2 mechanism.[6] Since the beginning of proton transfer from D-Glu was already observed in replica 5, no energy acyl-phosphate minimum comparable to replica path **1** was present in this pathway.

Following the initial formation of the acyl-phosphate intermediate the proton transfer reaction took place. Between replicas 5 and 7 the proton moved from the D-Glu amine to the oxygen of the γ-phosphate. According to energy analysis (see Fig. 8) this proton transfer was energetically highly demanding, as a value of 45 kcal/mol accounts for the transition barrier. This finding indicated that, due to significantly higher values of activation energy than normally expected for the enzyme-catalyzed processes, such proton transfer during the formation of tetrahedral intermediate is highly improbable. During the proton transfer the D-Glu moiety remained out of the covalent bonding region, ranging between 2.8 and 2.5 Å. The final formation of the tetrahedral intermediate **2** is depicted by replicas 9 through 15 where D-Glu moved towards the UMA C22 carbon atom forming the C—N bond. From an energetic perspective the C—N bond formation depicted in Figure 8 is a highly spontaneous process. However, as a strong H-bond interaction between a proton on γ-phosphate and the β-ATP phosphate oxygen is formed concurrently to the formation of a C—N bond (shown in supplementary material) the actual energy associated with the C—N bond formation could not be evaluated precisely.

Replica path 3

Reaction pathway **3** (**RPATh 3**) provided an atomistic picture of the reaction mechanism where the deprotonation of D-Glu was assisted by the nitrogen of His183. In the original scheme of the MurD mechanism, the role of His183 as a potential proton acceptor was considered only during the dissociation of the γ-phosphate from the tetrahedral intermediate due to its rather remote position (4.2 Å) deduced from the product UMAG in the crystal structure 4UAG.[6] Our optimized starting structures **I–III** agreed with these findings since the distances between His183 and the D-Glu amine ranged between 4.9–5.1 Å (Table I). Although the tetrahedral intermediate **3** was energetically significantly less favorable than the starting

Table IV

Variation of Important Bond Lengths (in Å) Along the Reaction Pathway Versus Replica Step Number in the Optimized QM/MM Replica Path RPATh 2

Reaction path step	PC (ATP)-O19 (UMA) (Å)	PC (ATP)-O3B (ATP) (Å)	N (D-Glu)-C22 (UMA) (Å)	H (D-Glu)-O1C (ATP) (Å)
1	2.76	1.79	3.09	3.58
2	2.55	1.97	3.14	3.54
3	2.32	2.22	3.17	3.54
4	2.12	2.48	3.11	3.28
5	1.97	2.70	3.00	2.87
6	1.85	2.85	2.87	2.10
7	1.77	2.95	2.72	1.17
8	1.71	3.02	2.50	0.95
9	1.67	3.06	2.19	0.98
10	1.64	3.08	1.89	0.98
11	1.63	3.10	1.67	0.99
12	1.62	3.12	1.57	0.99
13	1.62	3.18	1.54	1.00
14	1.62	3.28	1.55	1.01
15	1.61	3.42	1.58	1.02

Column 2: distance between the reacting γ-phosphate atom and the UMA terminal oxygen, Column 3: distance between the bond-breaking γ-phosphate and β-phosphate of ATP, Column 4: distance between the reacting terminal carboxylic UMA carbon and the amine nitrogen of D-Glu. Column 5: distance between the reacting D-Glu hydrogen and the ATP γ-phosphate oxygen involved in the proton transfer reaction.

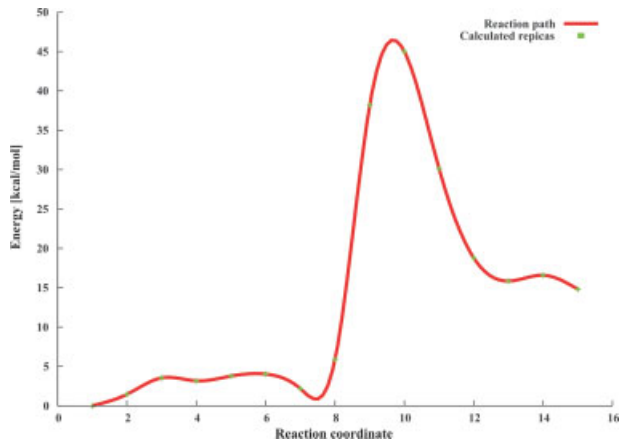

Figure 9

Energy diagram for the QM/MM optimized reaction pathway **RPATh 3** describing energetics along the reaction coordinate during the transformation of starting structure **III** to tetrahedral reaction intermediate **3**. [Color figure can be viewed in the online issue, which is available at www.interscience.wiley.com.]

structure **III**, we were still interested in evaluating this reaction mechanism using the QM/MM replica path approach since it provided an activation energy required for the proton transfer and substrates reacting order.

The QM/MM replica path **3** energy profile is depicted in Figure 9. Monitored distances presented in Table V indicated that during the first eight replicas no covalent bonds between the reacting species can be observed. Distance between D-Glu and UMA ranged between 3.0 and 2.7 Å and for the ATP and UMA distance values between 2.8 and 2.6 Å were observed. In these replicas D-Glu was positioned for a subsequent proton transfer reaction. The observed energy rise of between 3 and 4 kcal/mol agreed with the expected energy fluctuations associated with molecular conformational changes. The proton transfer was found to be a two-stage procedure, which was no surprise considering the initial distance between D-Glu and its proton acceptor—His183. In the first phase, the D-Glu proton transfer to the terminal UMA carboxylic oxygen was observed. This transfer was associated with a large energy rise that resulted in the transition state with activation energy of 45 kcal/mol in replica 10. In the second phase, the proton transfer to NE2 of His183 in replica 11 took place, lowering the energy of the system by ~15 kcal/mol. As in case of reaction path **2** the calculated activation barrier did not correspond to the enzymatic activation energies, indicating that in such a geometry of the MurD system, the proton transfer during the tetrahedral intermediate formation is highly unlikely. Both studied cases where the proton transfer was modeled concurrent with the tetrahedral intermediate formation resulted in high activation barriers. The replica path additional energy terms, which enable reaction pathway generation, do not constrain particular atoms directly and thus do not predetermine the movement along the reaction coordinate. Therefore, potential overestimation of the proton transfer energy barrier arising solely due to the utilization of the RPATh method can be ruled out. These results suggested that in MurD enzymatic reaction, the D-Glu residue most likely enters the amide bond forming reaction as a free base. The deprotonation mechanism of D-Glu moiety is presently unknown. Potential

Table V

Variation of Important Bond Lengths (in Å) Along the Reaction Pathway Versus Replica Step Number in the Optimized QM/MM Replica Path RPATh 3

Reaction path step	PC (ATP)-O19 (UMA) (Å)	PC (ATP)-O3B (ATP) (Å)	N (D-Glu)-C22 (UMA) (Å)	H (D-Glu)-O20 (UMA) (Å)	H (D-Glu)-NE2 (HIS183) (Å)
1	2.77	1.79	3.08	2.45	4.36
2	2.82	1.79	3.19	2.58	4.52
3	2.90	1.78	3.32	2.63	4.66
4	2.99	1.77	3.40	2.57	4.75
5	3.05	1.75	3.40	2.41	4.77
6	3.05	1.74	3.33	2.19	4.69
7	2.96	1.75	3.20	1.97	4.52
8	2.79	1.82	3.02	1.68	4.13
9	2.59	1.89	2.89	1.00	3.18
10	2.39	2.17	2.79	1.02	2.02
11	2.16	2.48	2.69	1.90	1.10
12	1.92	2.85	2.56	2.20	1.01
13	1.77	3.17	2.36	2.34	1.02
14	1.72	3.40	2.02	2.48	1.03
15	1.69	3.57	1.64	2.63	1.03

Column 2: distance between the reacting γ-phosphate atom and the UMA terminal oxygen, Column 3: distance between the bond-breaking γ-phosphate and β-phosphate oxygen of ATP, Column 4: distance between the reacting terminal carboxylic UMA carbon and the amine nitrogen of D-Glu. Column 5: distance between the reacting D-Glu hydrogen and the UMA terminal carboxylic oxygen O20 involved in the proton transfer reaction, Column 6: distance between the reacting D-Glu hydrogen and the His183 NE2 nitrogen involved in the proton transfer reaction.

explanation that might lead to a reduction of the high energy barriers observed in the studied proton transfer reactions would be the consideration of a water molecule playing a mediator role between the amino acid and its proton acceptor. Even in the postulated MurD mechanism,[6] the W600 crystal water is mentioned as possibly playing a role in the enzyme mechanism by orienting and stabilizing the D-Glu moiety. However, the uncertainty of the actual crystal water positions at the time the reaction commences and the fact that in our study D-Glu moiety was inserted into its active site by modeling makes any further investigation highly speculative.

Formation of covalent bonds between reacting substrates was described by replicas 11–15. A clear sequential reacting order was again observed in agreement with the proposed ligase kinetic mechanism.[7,8] With the onset of proton transfer in replica 9, the γ-phosphate PC atom breaks a covalent bond with the β-ATP phosphate oxygen and moves within the UMA O19 covalent binding distance of 1.9 Å (replica 12), which is similar to the distances of the acyl-phosphate intermediates previously discussed. D-Glu was located at 2.6 Å, still out of the covalent bonding distance. The energy rise associated with the proton transfer hindered the energy feature of the bi-pyramidal transition state. In replicas 13–15 the C—N bond formation resulted in the tetrahedral intermediate **3**.

CONCLUSIONS

This computational study represents an initial attempt to gain insight into the tetrahedral intermediate formation catalyzed by the bacterial MurD enzyme. This reaction is part of an enzymatic mechanism ultimately leading to a new amide bond formation. In the scope of this study three previously proposed mechanisms[6] leading to this intermediate were studied. A comparison with the postulated bacterial ligase kinetic mechanism[7,8] and available structural data[6] served as a benchmark to validate our results. The caveat must be issued that the bonding process itself, also determined by kinetic studies, was not possible to model simultaneously with the QM/MM reaction modeling and we are aware that in this respect, the constructed starting structure and the model itself represent a simplification of the MurD state during the reaction.

QM/MM minimizations resulted in starting structures **I–III**, which provided the geometries of the MurD system prior to an enzymatic reaction. The obtained configurations displayed a less favorable hydrogen bond pattern between D-Glu and its active site as observed for the product UMAG in the 4UAG crystal structure due to the presence of a repulsive interaction between side chain of Lys319 and a magnesium ion located between β- and γ-phosphate of ATP in a "classical magnesium binding site," obstructing Phe422 to adopt the favorable helical conformation. Such a hydrogen bond pattern was not observed in the 4UAG crystal structure, apparently due to the absence of this magnesium ion since magnesium was not included in the crystallization medium yielding this crystal structure.[6]

The two-stage QM/MM restrain-distance minimization provided geometries of tetrahedral intermediates **1–3**. Our results indicated that beside magnesium ions and Lys115, which facilitate the phosphate transfer,[6] water molecules play an important role in the stabilization of the formed acyl-phosphate intermediate. Energetic comparisons of tetrahedral intermediates **1–3** to their starting structures revealed that pairs **1** and **2** are energetically comparable. In the case of tetrahedral intermediate **3** with a proton located on His183, an endothermic nature of this reaction was suggested.

The QM/MM replica path method was successfully applied to chart the enzymatic reaction pathways between the pairs of QM/MM optimized structures. All optimized pathways are in line with a sequential reaction mechanism, displaying first the formation of a covalent acyl-phosphate intermediate and the subsequent formation of the C—N bond. Proton transfer to either the γ-phosphate of ATP or the nitrogen of His183 was found to be energetically too demanding to fit in the normal energy scope of reactions catalyzed by enzymes. This suggested that the D-Glu moiety most likely enters the enzyme reaction in its deprotonated form obtained by currently unidentified mechanism. In this respect our study established that the reaction mechanism **1** (**RPATh 1**) proposed by Dideberg and co-workers[6] would be the most probable mechanism.

The precise geometry of the tetrahedral intermediate is unknown and is largely derived from the efficiency of the identified transition state inhibitors. Therefore the unexpected rise in energy during the C—N bond formation in the deprotonated reaction pathway **1** can indicate that either some additional event, for example a second proton transfer, must occur together with the C—N bond formation or that a water molecule, which would hinder the C—N formation, is a reason for this observation. These questions will be considered in our future studies. We aspire that this work, together with our dynamic models of binding and C-terminal domain movements of MurD,[17] will contribute to a deeper understanding of these fascinating bacterial enzymes and supply novel information for advances in the design of novel antibacterials.

ACKNOWLEDGMENT

The authors thank Dr. Urban Borštnik for critical reading of the manuscript.

REFERENCES

1. Vollmer W, Blanot D, de Pedro MA. Peptidoglycan structure and architecture. FEMS Microbiol Rev 2008;32:149–167.
2. van Heijenoort J. Recent advances in the formation of the bacterial peptidoglycan monomer unit. Nat Prod Rep 2001;18:503–519.
3. Smith CA. Structure, function and dynamics in the mur family of bacterial cell wall ligases. J Mol Biol 2006;362:640–655.
4. Brown ED, Wright GD. New targets and screening approaches in antimicrobial drug discovery. Chem Rev 2005;309:759–774.
5. Silver LL. Does the cell wall of bacteria remain a viable source of targets for novel antibiotics? Biochem Pharmacol 2006;71:996–1005.
6. Bertrand JA, Auger G, Martin L, Fanchon E, Blanot D, Le Beller D, van Heijenoort J, Dideberg O. Determination of the MurD mechanism through crystallographic analysis of enzyme complexes. J Mol Biol 1999;289:579–590.
7. Anderson MS, Eveland SS, Onishi HR, Pompliano DL. Kinetic mechanism of the *Escherichia coli* UDPMurNAc-tripeptide D-alanyl-D-alanine-adding enzyme: use of a glutathione S-transferase fusion. Biochemistry 1996;35:16264–16269.
8. Emanuele JJ Jr, Jin H, Yanchunas J, Jr, Villafranca JJ. Evaluation of the kinetic mechanism of *Escherichia coli* uridine diphosphate-*N*-acetylmuramate:L-alanine ligase. Biochemistry 1997;36:7264–7271.
9. Bouhss A, Dementin S, van Heijenoort J, Parquet C, Blanot D. MurC and MurD synthetases of peptidoglycan biosynthesis: borohydride trapping of acyl-phosphate intermediates. Methods Enzymol 2002;354:189–196.
10. Falk PJ, Ervin KM, Volk KS, Ho H-T. Biochemical evidence for the formation of a covalent acyl-phosphate linkage between UDP-*N*-acetylmuramate and ATP in the *Escherichia coli* UDP-*N*-acetylmuramate:L-alanine ligase-catalyzed reaction. Biochemistry 1996;35:1417–1422.
11. Meek TD, Johnson KA, Villafranca JJ. *Escherichia coli* glutamine synthetase. Determination of rate-limiting steps by rapid-quench and isotope partitioning experiments. Derivation of equations for isotope partitioning experiments for a terreactant enzyme. Biochemistry 1982;29:2158–2167.
12. Shi Y, Walsh CT. Active-site mapping of *Escherichia coli* D-Ala-D-Ala ligase by structure-based mutagenesis. Biochemistry 1995;34:2768–2776.
13. Hiratake J, Kato H, Oda J. Mechanism-based inactivation of glutathione synthetase by phosphinic acid transition-state analog. J Am Chem Soc 1994;116:12059–12060.
14. Seelig GF, Meister A. Glutathione biosynthesis; γ-glutamylcysteine synthetase from rat kidney. Methods Enzymol 1985;113:379–390.
15. Sheng Y, Sun X, She Y, Bognar AL, Baker EN, Smith CA. Structural and functional similarities in the ADP-forming amide bond ligase superfamily: implications for a substrate-induced conformational change in folylpolyglutamate synthetase. J Mol Biol 2000;302:427–440.
16. Bertrand JA, Fanchon E, Martin L, Chantalat L, Auger G, Blanot D, van Heijenoort J, Dideberg O. "Open" structures of MurD: domain movements and structural similarities with folylpolyglutamate synthetase. J Mol Biol 2000;301:1257–1266.
17. Perdih A, Kotnik M, Hodoscek M, Solmajer T. Targeted molecular dynamics simulation studies of binding and conformational changes in *E. coli* MurD. Proteins 2007;68:243–254.
18. Bouhss A, Dementin S, Parquet C, Mengin-Lecreulx D, Bertrand JA, Le Beller D, Dideberg O, van Heijenoort J, Blanot D. Role of the ortholog and paralog amino acid invariants in the active site of the UDP-MurNAc-L-alanine:D-glutamate ligase (MurD). Biochemistry 1999;38:12240–12247.
19. Zoeiby AE, Sanschagrin F, Levesque RC. Structure and function of the Mur enzymes: development of novel. Inhibitors Mol Microbiol 2003;47:1–12.
20. Tanner ME, Vaganay S, van Heijenoort J, Blanot D. Phosphinate inhibitors of the D-glutamic acid-adding enzyme of peptidoglycan biosynthesis. J Org Chem 1996;61:1756–1760.
21. McDermott AE, Creuzet F, Griffin RG, Zawadzke LE, Ye QZ, Walsh CT. Rotational resonance determination of the structure of an enzyme-inhibitor complex: phosphorylation of an (aminoalkyl)-phosphinate inhibitor of D-alanyl-D-alanine ligase by ATP. Biochemistry 1990;29:5767–5775.
22. Strancar K, Blanot D, Gobec S. Design, synthesis and structure-activity relationships of new phosphinate inhibitors of MurD. Bioorg Med Chem Lett 2006;16:343–348.
23. Humljan J, Kotnik M, Boniface A, Solmajer T, Urleb U, Blanot D, Gobec S. A new approach towards peptidosulfonamides: synthesis of potential inhibitors of bacterial peptidoglycan biosynthesis enzymes MurD and MurE. Tetrahedron 2006;62:10980–10988.
24. Kotnik M, Humljan J, Contreras-Martel C, Oblak M, Kristan K, Hervé M, Blanot D, Urleb U, Gobec S, Dessen A, Solmajer T. Structural and functional characterization of enantiomeric glutamic acid derivatives as potential transition state analogue inhibitors of MurD ligase. J Mol Biol 2007;370:107–115.
25. Cavalli A, Carloni P, Recanatini M. Target-related applications of first principles quantum chemical methods in drug design. Chem Rev 2006;106:3497–3519.
26. Warshel A, Levitt M. Theoretical studies of enzymic reactions. J Mol Biol 1976;103:227–249.
27. Field MJ, Bash PA, Karplus M. A combined quantum mechanical and molecular mechanical potential for molecular dynamics simulations. J Comput Chem 1990;11:700–733.
28. Eurenius KP, Chatfield DC, Brooks BR, Hodoscek M. Enzyme mechanisms with hybrid quantum and molecular mechanical potentials. I. Theoretical considerations. Int J Quantum Chem 1996;60:1189–1200.
29. Das D, Eurenius KP, Billings EM, Sherwood P, Chatfield DC, Hodoscek M, Brooks BR. Optimization of quantum mechanical molecular mechanical partitioning schemes: gaussian delocalization of molecular mechanical charges and the double link atom method. J Chem Phys 2002;117:10534–10547.
30. Monard G, Prat-Resina X, González-Lafont A, Lluch JM. Determination of enzymatic reaction pathways using QM/MM methods. Int J Quantum Chem 2003;93:229–244.
31. Woodcock HL, Hodošček M, Sherwood P, Lee YS, Schaefer HL III, Brooks BR. Exploring the quantum mechanical/molecular mechanical replica path method: a pathway optimization of the chorismate to prephenate Claisen rearrangement catalyzed by chorismate mutase. Theor Chem Acc 2003;109:140–148.
32. Woodcock HL III, Hodoscek M, Gilbert ATB, Gill PMW, Schaefer HF III, Brooks BR. Interfacing Q-Chem and CHARMM to perform QM/MM reaction path calculations. J Comput Chem 2007;28:1485–1502.
33. Woodcock HL, Hodoscek M, Brooks BR. Exploring SCC-DFTB paths for mapping QM/MM reaction mechanisms. J Phys Chem A 2007;111:5720–5728.
34. Lee YS, Pike VW, Hodoscek M. Identification of the transition states in the inversion of 1,4-benzodiazepines with the ab initio replica path method. J Phys Chem A 2008;112:1604–1611.
35. Czerminski R, Elber R. Reaction path study of conformational transitions in flexible systems: applications to peptides. J Chem Phys 1990;92:5580–5601.
36. Elber R, Karplus M. A method for determining reaction paths in large molecules: application to myoglobin. Chem Phys Lett 1987;139:375–380.
37. Walsh AW, Falk PJ, Thanassi J, Discotto L, Pucci MJ, Ho HT. Comparison of the D-glutamate-adding enzymes from selected gram-positive and gram-negative bacteria. J Bacteriol 1999;181:5395–5401.
38. Brooks BR, Bruccoleri RE, Olafson BD, States DJ, Swaminathen S, Karplus M. CHARMM: a program for macromolecular energy. Minimization, and dynamics calculations. J Comput Chem 1983;4: 187–217.
39. Schmidt MW, Baldridge KK, Boatz JA, Elbert ST, Gordon MS, Jensen JH, Koseki S, Matsunaga N, Nguyen KA, Su S, Windus

TL, Dupuis M, Montgomery JA. General atomic and molecular electronic structure system. J Comput Chem 1993;14:1347–1363.
40. Yang W, Parr RG. Density functional theory of atoms and molecules. New York: Oxford University Press; 1986.
41. MacKerell AD Jr, Bashford D, Bellott M, Dunbrack RL Jr, Evanseck JD, Field MJ, Fischer S, Gao J, Guo H, Ha S, Joseph-McCarthy D, Kuchnir L, Kuczera K, Lau FTK, Mattos C, Michnick S, Ngo T, Nguyen DT, Prodhom B, Reiher WE III, Roux B, Schlenkrich M, Smith JC, Stote R, Straub J, Watanabe M, Wiorkiewicz-Kuczera J, Yin D, Karplus M. All-atom empirical potential for molecular modeling and dynamics studies of proteins. J Phys Chem B 1998;102:3586–3616.
42. MacKerell AD Jr, Feig M, Brooks CL, III. Extending the treatment of backbone energetics in protein force fields: limitations of gas-phase quantum mechanics in reproducing protein conformational distributions in molecular dynamics simulations. J Comput Chem 2004;25:1400–1415.
43. Foloppe N, MacKerell AD Jr. All-atom empirical force field for nucleic acids. I. Parameter optimization based on small molecule and condensed phase macromolecular target data. J Comput Chem 2004;25:86–104.
44. MacKerell AD Jr, Banavali NK. All-atom empirical force field for nucleic acids. II. Application to molecular dynamics simulations of DNA and RNA in solution. J Comput Chem 2004;25:105–120.
45. Borštnik U, Hodošček M, Janežič D. Improving the performance of molecular dynamics simulations on parallel clusters. J Chem Inf Comput Sci 2004;44:359–364.
46. Jorgensen WL, Chandrasekhar J, Madura JD, Impey RW, Klein ML. Comparison of simple potential functions for simulating liquid water. J Chem Phys 1983;79:926–935.
47. Humphrey W, Dalke A, Schulten K. VMD: visual molecular dynamics. J Mol Graph 1996;14:33–38.
48. Gnuplot 4.0., An interactive plotting program, © Copyright T. Williams & C. Kelley. 2004. http://www.gnuplot.info.
49. Mol CD, Brooun A, Dougan DR, Hilgers MT, Tari LW, Wijnands RA, Knuth MW, McRee DE, Swanson RW. Crystal structures of active fully assembled substrate- and product-bound complexes of UDP-*N*-acetylmuramic acid:L-alanine ligase (MurC) from *Haemophilus influenzae*. J Bacteriol 2003;185:4152–4162.